

*Biochemistry*. Author manuscript; available in PMC 2013 August 28.

Published in final edited form as:

Biochemistry. 2010 October 5; 49(39): 8554-8563. doi:10.1021/bi100913v.

# Substitution of Ala for Tyr567 in RB69 DNA Polymerase Allows dAMP and dGMP To Be Inserted Opposite Guanidinohydantoin<sup>†</sup>,,‡

**Jeff Beckman**<sup>‡</sup>, **Mina Wang**<sup>‡</sup>, **Gregor Blaha**, **Jimin Wang**<sup>\*</sup>, and **William H. Konigsberg**<sup>\*</sup> Department of Molecular Biophysics and Biochemistry, Yale University, New Haven, Connecticut 06520-8024

# Abstract

Continuous oxidative damage inflicted on DNA produces 7,8-dihydro-8-oxoguanine (8-oxoG), a commonly occurring lesion that can potentially cause cancer by producing  $G \to T$  transversions during DNA replication. Mild oxidation of 8-oxoG leads to the formation of hydantoins, specifically guanidinohydantoin (Gh) and spiroiminodihydantoin (Sp), which are 100% mutagenic because they code almost exclusively for the insertion of dAMP and dGMP (coding for  $G \to T$  and  $G \to C$  transversions, respectively). The wild type (wt) pol  $\alpha$  family DNA polymerase from bacteriophage RB69 (RB69pol) inserts dAMP and dGMP with low efficiency when situated opposite Gh. In contrast, the RB69pol Y567A mutant inserts both of these dNMPs opposite Gh with > 100-fold higher efficiency than wt. We now report the crystal structure of the "closed" preinsertion complex for the Y567A mutant with dATP opposite a templating Gh (*R*-configuration) in a 13/18mer primer-template (P/T) at 2.0 Å resolution. The structure data reveals that the Y to A substitution provides the Nascent base-pair Binding Pocket (NBP) with the flexibility to accommodate Gh by allowing G568 to move toward the minor groove in the P/T. Thus, Gh is rejected as a templating base by wt RB69pol because G568 is inflexible, preventing Gh from pairing with the incoming dATP or dGTP base.

The average human cell acquires approximately 6000 DNA lesions per day due to oxidative damage by reactive oxygen species (ROS) (1). Guanine has the lowest oxidation potential of the four natural bases, and is readily oxidized to 7,8-dihydro-8-oxoguanine (8-oxoG) (2). As a templating base, 8-oxoG codes for insertion of dCMP and dAMP (Fig. 1*A*).  $G \rightarrow T$  transversions, which have been linked to cancer, aging, and other deleterious diseases, occur if a DNA polymerase mistakenly inserts dAMP opposite 8-oxoG that is in the *syn* conformation (*syn*-8-oxoG) (3–5).

8-oxoG has a lower oxidation potential than G (6–8), and can be oxidized further forming a variety of lesions, such as guanidinohydantoin (Gh) and spiroiminodihydantoin (Sp) (Fig. 1B) (9, 10). These lesions can form a base-pair between their hydantoin rings and dATP, although the most stable conformation of Gh is "high-syn", which would create a slightly "buckled" base-pair with dATP (Fig. 1C) (11, 12). (For reference, figure 1D shows the numbering scheme for Gh, (13).) Gh and Sp do not base-pair with dCTP, so these lesions are more mutagenic than 8-oxoG (14). Burrows et al. (15–17) confirmed this when they found

<sup>&</sup>lt;sup>†</sup>Supported by a grant from USPHS GM 063276

<sup>&</sup>lt;sup>‡</sup>With regard to author contributions, J.B. determined the kinetic parameters, M.W. crystallized and determined the structure of the RB69pol–Gh ternary complex, G.B. collected data at APS, and J.B., J.W., and W.H.K. helped to interpret the data, designed experiments, and contributed to writing the paper.

<sup>\*</sup>Address correspondence to: Prof. William H. Konigsberg, Dr. Jimin Wang, Department of Molecular Biophysics and Biochemistry, Yale University, SHM CE-14, New Haven, CT 06520-8114, Telephone: (203) 785-4599, Fax: (203) 785-7979, William.konigsberg@yale.edu, jimin.wang@yale.edu.

Authors contributed equally to this work

that the Klenow fragment (KF) could insert dAMP, but not dCMP, opposite Gh and Sp. dGMP was also inserted opposite these lesions, albeit with lower efficiency than dAMP. It has been proposed that the efficiency of dGMP insertion is higher than that of dCMP or dTMP because a G:Gh base-pair is closer to "ideal" Watson-Crick geometry (11).

Misinsertion of dGMP gives rise to  $G \rightarrow C$  transversions which have been identified with high frequency in cells that have been transformed with plasmids exposed to the following oxidizing agents: (i) UV light (18, 19); (ii) hydrogen peroxide (20); (iii) methylene blue plus light (21) or; (iv) singlet oxygen (endoperoxide) (22). Although Gh has not been detected *directly* in cancer cells with elevated levels of these mutations, e.g., some head and neck carcinoma cell lines (23), hydantoins like Gh are one of only a few known DNA adducts formed by oxidation to code for  $G \rightarrow C$  transversions, linking Gh and Sp to human cancer (24). This link was strengthened by the findings that Gh and Sp were substrates for removal by the mammalian glycosylases NEIL1, NEIL2, and hNEIL1 (25–27), suggesting that DNA repair pathways have evolved to recognize and excise hydantoins.

Unlike the situation with KF, Gh blocked replication by family B polymerases such as RB69pol, calf thymus DNA pol  $\alpha$ , and human DNA pol  $\beta$  (11, 17). A recently solved crystal structure of RB69pol in complex with DNA containing Gh revealed that the mechanism by which RB69pol rejected Gh as a templating base was by flipping it away from contact with an incoming dNTP and into the major groove (11). Because Gh has high mutagenic potential, and because RB69pol has a relatively high degree of sequence similarity to the human pols  $\alpha$  and  $\delta$  (28), it was of interest to determine why wt RB69pol rejects Gh as a templating base. To do so, we would have to trap Gh in the templating position in a ternary complex.

We recently reported that the RB69pol Y567A mutant increased the insertion efficiency of dAMP opposite 8-oxoG by > 2 orders of magnitude relative to wt (29). Figure 2 illustrates the location of Y567 in relation to the nascent base-pair and other NBP residues. Replacement of the Y567 side chain with a methyl group increased the flexibility of the neighboring G568 residue, allowing it to readjust its position to accommodate, and stabilize, syn-8-oxoG (29). Because Gh has similar structural and chemical features as syn-8-oxoG in regions of the molecule that would closely contact G568 and the incoming dATP base, we predicted that the Y567A mutant would also be able to insert dAMP opposite Gh with high efficiency. This prediction was confirmed when we found that dAMP opposite Gh was incorporated with > 200-fold greater efficiency than wt. In addition, the insertion efficiency of dGMP opposite Gh by the Y567A mutant increased by 100-fold relative to wt. To provide the structural basis for efficient utilization of Gh as a templating base by the Y567A mutant, and in an attempt to understand why wt RB69pol cannot bypass Gh, we determined the crystal structure of the ternary complex of the Y567A mutant with dATP opposite a templating Gh at 2.0 Å resolution. Our kinetic and structural data has provided insights into how dATP and dGTP are utilized by the Y567A mutant when paired opposite Gh, and has led to a deeper understanding of base selectivity, as discussed below.

#### **MATERIALS AND METHODS**

#### **Materials**

Materials and reagents were of the highest quality commercially available. dNTPs were purchased from Roche (Burgess Hill, UK), T4 polynucleotide kinase was purchased from New England Biolabs (Ipswich, MA), and  $[\gamma$ -32P]ATP was purchased from MP Biomedicals (Irvine, CA).

#### **Enzymes**

Wild-type RB69pol and the Y567A mutant, in an exonuclease-deficient background (D222A and D327A), were over-expressed in *Escherichia coli*, purified, and stored as previously described (30).

#### **DNA Substrates**

Sequences of primer-templates (P/T) used in this study are shown in Table 1. Oligonucleotides, with the exception of those containing Gh, were synthesized at the Keck facilities (Yale University). Oligonucleotides containing 8-oxoG were oxidized with Ir (IV) to convert 8-oxoG to the two diastereoisomers of Gh as described previously (15, 16). Primers were labeled on the 5'-end with  $^{32}$ P using T4 polynucleotide kinase and  $[\gamma$ -32P]ATP (except when used for crystallography) and annealed to unlabeled templates as previously described (31, 32).

### **Chemical Quench Experiments**

Rapid chemical quenching experiments were performed at 23°C with a buffer solution of 66 mM Tris-HCl (pH 7.4) using a Kintek RFQ-3 instrument. For  $k_{pol}$  and  $K_{d,app}$ determinations, single-turnover conditions were used with a 10-fold excess RB69pol over P/ T. Briefly, enzyme and P/T from one syringe were rapidly mixed with Mg<sup>2+</sup> and various [dNTP]s from the other syringe for times ranging from 5 ms to 1 min. For reactions that required longer times, experiments were performed manually on the bench-top. For most reactions, the rate of phosphoryl transfer was too low to obtain kinetic parameters in the presence of a trap, e.g. cold dsDNA or heparin. However, in the case of dAMP insertion opposite Gh by the Y567A mutant, where the rate of chemistry was orders of magnitude faster than the rate of DNA release, 10x [cold P/T] over [enzyme] was used to ensure that single turnover conditions were met (Table 2). The final concentrations after mixing were 1 μM enzyme, 90 nM <sup>32</sup>P-labeled P/T, and 10 mM Mg<sup>2+</sup>. Reaction mixtures were quenched with 0.5 M EDTA (pH 8.0). Substrates and products were separated by PAGE (19:1% (w/v) acrylamide:bisacrylamide gels containing 8M urea), visualized using a STORM imager (Molecular Imaging), and quantitated using Imagequant (GE Healthcare) and GraphPad Prizm.

#### **Data Analysis**

The amount of product formed versus time for each [dNTP] were fitted by non-linear regression to the general form of Equation 1 to obtain *observed* rates of product formation,  $k_{\text{obs}}$ :

$$Y = \sum_{i=1}^{n} A_i e^{-k_i t} + C \quad \text{Eq. 1}$$

where Y is the concentration of the DNA product formed during the reaction, C is the offset constant,  $A_i$  the observed amplitude of product formation, and  $k_i$  the observed rate constant. The kinetic parameters  $k_{\text{pol}}$  (the rate of phosphoryl transfer) and  $K_{\text{d,app}}$  (defined as the [dNTP] at which the rate of phosphoryl transfer reaches 1/2  $k_{\text{pol}}$ ), were obtained by plotting  $k_{\text{obs}}$  versus [dNTP] to Equation 2:

$$k_{\text{obs}} = \frac{k_{\text{pol}}[\text{dNTP}]}{K_{d,\text{app}} + [\text{dNTP}]}$$
 Eq. 2

where  $k_{\rm obs}$  represents the observed rate at a given [dNTP]. Note that the  $K_{\rm d,app}$  values are not ground-state dissociation constants for dNTP binding. This is because the observed

[dNTP]-dependence of rates of product formation is affected by steps such as the reversible conformational change that occurs subsequent to dNTP binding but prior to phosphoryl transfer.

# Crystallization of RB69pol Y567A mutant ternary complexes with dATP:Gh

 $D_{GH}^{dd}$  was used for crystallization (Table 1). The primer was dideoxy-terminated to prevent nucleotide incorporation. The RB69pol Y567A mutant (110  $\mu M$  final concentration) was mixed with an equimolar ratio of freshly annealed  $D_{GH}^{dd}$ . dATP was then added to a final concentration of 3.7 mM. Using micro-batch vapor-diffusion methods, a solution of 150 mM CaCl<sub>2</sub>, 15%(w/v) PEG 350 monomethyl ether (MME), and 100 mM Na Cacodylate (pH 6.5) was mixed with an equal volume of the Y567A:  $D_{GH}^{dd}$ :dATP complex. Crystals typically grew in 3 days at 20°C with dimensions of about 70 $\mu m \times 50 \mu m \times 50 \mu m$ . Crystals were transferred from the mother liquor to a cryoprotectant/precipitant stabilization solution containing 20% (w/v) PEG 350 MME, 100 mM CaCl<sub>2</sub>, and 100 mM Na Cacodylate (pH 6.5), then to the stabilization solution with PEG 350 increased to 30% (w/v) as a cryoprotectant prior to freezing in liquid nitrogen.

#### Data collection, structure determination, and refinement

X-ray diffraction data were collected using synchrotron radiation sources at beamline X25 at Brookhaven National Laboratory (NSLS) (Upton, NY) at a wavelength of 1.10000 Å and at 110 K using synchrotron radiation sources. The crystal belonged to the orthorhombic space group  $P2_12_12_1$  with different unit cell parameters (Table 3). Data were processed using the HKL2000 program suites (33).

The structure was solved by molecular replacement using AMORE, starting with the pol structure from the ternary complex of wt RB69pol without the P/T duplex or dNTP (34), and refined using REFMAC5 (35, 36). The P/T duplex and dNTP were built into electron density maps using the program COOT (37). The incoming dATP binds two Ca<sup>2+</sup> ions at the A and B metal ion sites, as was observed previously (34). The structure of Gh was derived from the PDB entry 3L8B, which contains a Gh nucleotide residue in the template strand (11). Structure refinement statistics are summarized in Table 3. Figures obtained from the crystal structures were made using the program Ribbons (38).

#### PDB accession numbers

Coordinates and structure factors for the Y567A mutant dATP:Gh ternary complex structure have been deposited in the Protein Data Bank under accession code 3NAE.

## **RESULTS**

#### Insertion of dNMPs opposite Gh by wild type RB69pol and the Y567A mutant

Overall, bypass of a Gh lesion by a replicative DNA pol is much more mutagenic than bypass of 8-oxoG, because Gh does not base-pair with dCTP (Fig. 3*A*) (9). Steady-state kinetic analysis of dNMP incorporation opposite Gh by wt RB69pol showed that this lesion allows insertion of dATP and dGTP, but with very low efficiency (11). Under pre-steady-state conditions, insertion of dAMP and dGMP opposite Gh by wt RB69pol occurred at efficiencies of  $1.5\times10^{-3}$  and  $5.7\times10^{-5}$   $\mu$ M $^{-1}$  s $^{-1}$ , respectively, favoring insertion of dAMP over dGMP by 25-fold. These efficiencies are still ~ 3000-fold lower than insertion of correct dNMPs by wt opposite an undamaged templating base (Table 2) (39).

What prevents incorporation of dAMP and dGMP opposite Gh by wt RB69pol? We had previously found that the Y567A mutant increased the incorporation efficiency of dAMP opposite *syn*-8-oxoG by 3 orders of magnitude relative to wt (29). We speculated that this

may have occurred in part because the Y to A substitution provides G568 with the flexibility to accommodate syn-8-oxoG, as well as its ability to form a potentially stabilizing hydrogen bond between the Ca-hydrogen atom of G568 and the O-8 carbonyl oxygen of 8-oxoG (29). As with syn-8-oxoG, Gh contains a carbonyl oxygen that is close enough to the Ca hydrogen of G568 to form a hydrogen bond. This suggested that Y567A would also increase the efficiency of dAMP incorporation opposite Gh as it does with dAMP opposite 8-oxoG. Under pre-steady-state conditions in the presence of cold DNA trap (see Experimental Procedures), the progress curves for the Y567A mutant inserting dAMP opposite Gh occurred in two phases: a fast phase accounting for approximately 80% of the total product formed and a slow phase responsible for the remainder. Because Gh exists as a racemic mixture of diastereoisomers, differing only at the C-4 carbon that links the hydantoin ring with the guanidinium group (Fig. 1D) (11), the biphasic curves may represent dAMP insertion opposite each of the two forms. Analysis of the "fast" phase revealed that dAMP insertion efficiency was 200 times greater than that observed with wt RB69pol (Fig. 3). The  $k_{\text{pol}}$  is similar to the rate of insertion of dCMP opposite G (Table 2) (39). dGMP incorporation efficiency, when opposite Gh, by the Y567A mutant also increased 100-fold over wt (Table 2).

#### Extension past A:Gh and G:Gh base-pairs

Bypass of A:Gh and G:Gh terminal base-pairs by wt RB69pol and the Y567A mutant was very inefficient (10<sup>5</sup>- to 10<sup>6</sup>-fold lower than extension past normal W-C base-pairs) (Table 4). By comparison, the bypass efficiency of terminal C:8-oxoG and A:8-oxoG base-pairs by both wt RB69pol and the Y567A mutant (29) was at least 3 orders of magnitude more efficient than extension past A:Gh and G:Gh base-pairs (Table 4).

## Bypass of other template analogs

For further insight into why the Y567A mutant efficiently bypassed 8-oxoG but not Gh, we examined the ability of wt RB69pol and the Y567A mutant to bypass thymine glycol (Tg) and 1,3-diaza-2-oxophenoxazine (tC $^{\rm o}$ ) (Fig. 4). Previous results had shown that wt RB69pol bypass of Tg was very inefficient, but that bypass of tC $^{\rm o}$  by the related B family human pol  $\alpha$  was highly efficient (40, 41). Both wt RB69pol and the Y567A mutant rapidly inserted dAMP opposite Tg, and dGMP opposite tC $^{\rm o}$ , and both pols rapidly inserted the next correct dNMP (dTMP) past terminal G:tC $^{\rm o}$  and A:tC $^{\rm o}$  base-pairs, but only slowly extended past A:Tg and G:Tg base-pairs. In most cases, compared to wt, the Y567A mutant increased the rate of bypass by several-fold or more.

# Crystal structure of the Y567A mutant in complex with a Dideoxy P/T containing a templating Gh opposite dATP

To correlate kinetics with structure, we required high-quality crystals of RB69pol with a templating Gh. Recently, a crystal structure of wt RB69pol in complex with dP/T containing Gh was reported (11). Surprisingly, although Gh was expected to be in the templating position, it was flipped out into the major groove. Also, despite having been grown in a solution containing 10 mM ddATP under conditions that would allow phosphoryl transfer, no electron density was observed for an inserted ddAMP, and the polymerase remained in an "open" conformation (11). We have determined the structure of a ternary complex of the Y567A mutant with a templating Gh opposite dATP, at 2.0 Å resolution with an  $R_{\rm free}$  value of 23% (Table 3). In contrast to the reported wt RB69pol Gh complex, Gh in the Y567A mutant structure is paired opposite dATP in the "closed" conformation with the hydantoin ring of Gh forming a hydrogen bond between the N-7 of Gh and N-1 of dATP (Fig. 5). Although we predicted that the O-5 of Gh and N-6 of dATP to have the capability of forming an inter-base hydrogen bond, this did not occur. Instead, O-5 of Gh and N-6 of dATP form an indirect hydrogen bond mediated by an ordered water molecule (Fig. 5*A*).

The electron density of the guanidinium group of Gh was well resolved. As was the case in the wt binary structure, Gh, which has a chiral center at C-4 and exists as a mixture of *S*- and *R*-forms, was found exclusively in the *R*-configuration. (Computer modeling showed that if the *S*-configuration would have been captured instead, the guanidinium moiety would have pointed towards the helix P side-chains, which would force the 3'-template base of a nascent base-pair to "buckle" to avoid steric repulsion.)

For insight into the structural consequences of having a templating Gh in the NBP, we superimposed the palm domains of ternary complexes of wt with dCTP:dG and the Y567A mutant with dATP:Gh (Fig. 5*B*). The wt structure was determined at 1.8 Å resolution (Wang, M. manuscript in preparation). We observed that the incoming dATP was almost perfectly superimposed onto the incoming dCTP in the wt RB69pol structure, although the orientation of the glycosidic bond of the two incoming dNTPs differed slightly. The most significant changes in these structures were; (i) the backbone of G568 was retracted into the DNA minor groove by 0.8 Å, (ii) the side chain of K279 was displaced by 6.7 Å to avoid a steric clash with the guanidinium moiety of Gh, and; (iii) the vacated space, due to the Y567 to A substitution, was occupied by two ordered water molecules (data not shown).

#### DISCUSSION

To help counter the effects of oxidized DNA damage, it is important to understand the mechanism(s) by which DNA pols replicate DNA containing oxidized lesions like Gh. Recently, a wt RB69pol:P/T binary crystal structure was solved with the R-form of Gh at the P/T junction in the template strand (11). In contrast to the situation with the Y567A mutant, Gh shifted from the templating position into the major groove. However, wt RB69pol preferably inserts, albeit inefficiently, dAMP and dGMP opposite Gh, indicating that R-Gh rotates only infrequently into the templating position. Alternatively, only the S-form of Gh, which did not crystallize but is present in solution, can be positioned as a template base (11). Because R-Gh fits into the templating position nicely within the Y567A mutant closed ternary complex, and maintains preference for insertion of dAMP and dGMP opposite Gh, the likely mechanism utilized by the Y567A mutant to efficiently insert dAMP and dGMP is to increase the probability of repositioning Gh as the template base (Table 2) (Fig. 5A). What structural feature does the Y567A mutant provide so that Gh can occupy the templating position? The Y567 Ca is about 11.3 Å away from the guanidinium moiety, so the Y567 to A substitution cannot have a direct effect on the stability of Gh, i.e. by providing additional space in the NBP. Instead, the effect must be indirect. The loss of the phenolic side-chain of Y567 increases the flexibility of G568, allowing Gh to become stable as a templating base. Specifically, formation of a dATP:Gh pair in the Y567A mutant can occur because G568 can move ~ 0.8 Å into the DNA minor groove to provide the space needed for Gh to pair with the base of dATP (Fig. 5B). We had previously shown that the Y567A mutant is permissive for insertion of dAMP opposite syn-8-oxoG using the same mechanism (29). This increased flexibility also allows Gh to stabilize the dATP:Gh pair because the Ca hydrogen atom of G568 and O-8 of Gh are close enough for hydrogen bond formation.

Currently, we do not fully understand why the substitution of the phenolic side-chain of Y567 with a methyl group leads to more flexibility of G568. Because Y567 forms hydrogen bonds with Y391 and T587, and forms a close association with Y416, we suspect Y567 makes G568 rigid because Y567 is itself rigid. Thus, any, if not all, of the interactions formed between Y567 and other side-chains may contribute to the rigidity of G568. We are currently in the process of analyzing the appropriate mutants to determine which interactions between side-chains leads to increased G568 flexibility. Having a better understanding of how to increase the flexibility of active-site residues would have practical applications,

specifically in the field of protein engineering. In recent years, researchers have been polymerizing DNA with a variety of nucleotide modifications (e.g., (42–47)), with goals that include the expansion of the genetic code and novel nucleic acid therapeutics (48). Theoretically, mutants could be engineered to have the active-site flexibility for judicious, and efficient, incorporation of novel modifications into DNA.

Interestingly, despite the absence of stabilizing interactions between residues in the NBP and the guanidinium group of Gh, Gh is surprisingly well ordered, and surrounded by five water molecules in an extended hydration network (Fig. 5A). Numerous other ordered water molecules line the DNA major groove, including one mediating the interaction between O-5 of Gh and N-6 of dATP. This water molecule interacts with another water molecule in the major groove that binds to O-6 of the dG base that is 3' to Gh on the templating strand (Fig. 5A). With the exception of the mediation of water molecules between the nascent base-pair, dATP binding opposite Gh suggests "normal" solvation and W-C-like base-pairing. However, because the  $K_{d,app}$  of dAMP insertion is approximately 15-fold higher than would be expected for a W-C base-pair, it suggests that the apparent binding affinity of dATP is relatively low with the Y567A mutant (39) (Table 2). These kinetic observations correlate with the inability of the nascent base-pair to form two strong inter-base hydrogen bonds. Additionally, we have noted that the K279 side-chain has shifted away from the guanidinium group of Gh by 6.7 Å probably because of electrostatic repulsion (Fig. 5B). However, previous studies with the K279A mutant showed that K279 does not influence the insertion efficiency of dAMP opposite Gh (11). Despite the increase in  $K_{d,app}$  for dATP, the  $k_{\text{pol}}$  is very high for dAMP insertion (300 s<sup>-1</sup>), so presumably the dATP:Gh pair is still optimally aligned for phosphoryl transfer (Table 2), consistent with the observation that dATP opposite Gh in this complex is superimposed well with dCTP opposite dG in the ternary complex structure (Fig. 5B).

# The dGTP:Gh base-pair adopts a "wobble" configuration in the Y567A mutant ternary complex

It has been proposed that Gh pairs opposite G in a "wobble" configuration (49), where Gh acts like dT in terms of the inter-base hydrogen bonding pattern. Modeling and NMR structural studies of duplex DNA have shown that base-pairs adopt "wobble" configurations when inter-base hydrogen bonds have the potential to form, suggesting that "wobble" pairing represents a possible mechanism for misinsertion of dNMPs by DNA pols (e.g. (50– 53)). By increasing the volume of the NBP in RB69pol, Klentaq1, and Taq pol1 by sitedirected mutagenesis, dTMP insertion was 1 to 2 orders of magnitude more efficient opposite dG, suggesting that wt DNA pols use steric hindrance to prevent the formation of dTTP:dG "wobble" configurations (39, 54, 55). Specifically, the Y567A mutant inserts dTMP 40-fold more efficiently than does wt RB69pol. However, base-pairing of dTTP opposite dG with two hydrogen bonds would require a "wobble" configuration with the incoming base shifted into the DNA major groove, not downward into the space provided by the Y567 to A substitution. Thus, steric repulsion does not adequately explain how dTMP misinsertion opposite dG is prevented in wt pol. Instead, the more efficient insertion of dTMP opposite dG by the Y567A mutant is likely caused by the increased flexibility of G568, allowing the templating dG to shift into the DNA minor groove (Fig. 6A). In contrast, to obtain two inter-base hydrogen bonds between dGTP and Gh, an "inverted wobble" configuration would be required, with the dGTP base shifting into the DNA minor groove (Fig. 6B). In this case, a steric clash with Y567 would be a more probable explanation as to why the wt pol rejects dGTP opposite Gh. We have recently solved the structures of two ternary complexes of the Y567A mutant with dTTP:dG and dCTP:2-aminopurine (dCTP:dAP) mispairs and found that the base-pairs are in the "wobble" and "inverted wobble" configurations, respectively (Konigsberg, W; manuscript in preparation). The latter

configuration leads to the formation of two hydrogen bonds between dCTP and dAP with the base of dCTP shifted into the DNA minor groove and into the space provided by the Y567 to A substitution, just as we suspect happens with a dGTP:Gh pair (Wang, J. personal communication). Overall, the structural and kinetic data support our proposal that the dNTP or the templating base can readily be repositioned within the NBP of the Y567A mutant for formation of relatively stable mispairs.

# Extension past A:Gh and G:Gh base-pairs is blocked in both wt and the Y567A mutant

Previous studies have shown that DNA pols, with the exception of KF, extend primers beyond terminal base-pairs containing Gh with very low efficiency (11, 17). Overall, with wt RB69pol, this makes Gh a very poor template for dNMP insertion as well as a very poor base-pairing partner for further extension of the growing primer strand. Interestingly, although the Y567A mutant is able to efficiently insert dAMP opposite Gh relative to wt, it is only slightly better (3-fold) at inserting the next correct dNMP past a dAMP:Gh terminal base-pair than wt (Table 4). In contrast, dAMP: syn-8-oxoG and dCMP: anti-8-oxoG terminal base-pairs are efficiently extended past by the Y567A mutant, compared to wt, and this may provide an explanation for the Gh extension results (29). Modeling studies have shown that 8-oxoG in either the syn- or anti-orientations contain functional groups that would protrude into the pol cavity that holds the DNA duplex and would sterically clash with neighboring side-chains, e.g., W574 and N572 (Fig. 7A), so it is not surprising that wt RB69pol would be unable to efficiently bypass base-pairs containing 8-oxoG (29, 56). This proposal is supported by reports from the Kool, Kuchta, and Romesberg groups (57–61) who have shown, using nucleoside analogs, that terminal base-pairs have to adopt a W-C or similar geometry for efficient extension. The Y567A mutant may provide the flexibility for extension past protruding functional groups during DNA translocation through the pol active site by eliminating hydrogen bonds that would otherwise form a rigid network between Y567, Y391 and T578 (29, 62). Because of this putative flexibility, the dAMP:Gh and dAMP:syn-8-oxoG terminal base-pairs should be extended past with similar efficiency by the Y567A mutant. This is based on *In silico* modeling of A:Gh or A:syn-8-oxoG base-pairs superimposed onto the terminal base-pair (via the glycosidic bonds), which shows that similar steric clashes occur between Gh or 8-oxoG and its 5'-bridging phosphate group (Fig. 7B,C) (29). However, the aforementioned terminal dAMP:Gh base-pair is extended poorly relative to dAMP:syn-8-oxoG. This may be explained if we were to assume that Gh prefers to form a dAMP: high-syn-Gh configuration when in the terminal base-pairing position. This configuration is predicted to be the most stable for Gh in DNA alone (11). A dAMP: highsyn-Gh base-pair would create more distortion than dAMP:Gh pair because the former would "buckle" (see Fig. 1 C for a probable configuration of a dAMP: high-syn-Gh basepair). This distortion would be expected to cause steric repulsion with the adjacent nascent base-pair, and would lead to destabilization that would favor dNTP dissociation over phosphoryl transfer. Predictably, this repulsion could not be relieved by the additional flexibility of side-chains in the Y567A mutant that protrude into the DNA minor-groove.

Additional evidence to support the idea that W-C or similar geometry is required for efficient bypass is provided by the observation that the Y567A mutant rapidly extends past a G:tC<sup>o</sup> terminal base-pair, but much more slowly past an A:Tg base-pair (Fig. 4). Unlike tC<sup>o</sup>, Tg, as with "*High-syn*"-Gh, distorts the terminal base-pair plane in a fashion that prevents the 3′-templating base from forming a stable interaction with the dNTP (40). Presumably, bypass of tC<sup>o</sup> is efficient because tC<sup>o</sup> can form a W-C base-pair, albeit with extra bulk protruding into the DNA major groove (Fig. 4*B*) (41).

In summary, wt RB69pol is able to prevent misinsertion largely because it possesses a rigid DNA minor-groove "wall", comprising Y567 and G568, that not only prevents misinsertion of dAMP opposite Gh, but also misinsertion of dNMPs that could form Py:Pu, Pu:Py, or

dGTP:Gh "wobble" pairs. Simply by substituting Y567 with Ala, fidelity drops dramatically because G568 now becomes flexible, allowing for either dNTP bases and/or templating bases, including Gh, to shift into the DNA minor groove by displacing G568 into the pol interior. These results underscore the need to better elucidate the interrelationships between amino acid side-chains within the NBP and bound substrates if we are to understand the mechanism(s) by which DNA pols achieve high fidelity replication.

#### **ABBREVIATIONS**

Gh GuanidinohydantoinSp spiroiminodihydantoin8-oxoG 7,8-dihydro-8-oxoguanine

Tg thymine glycol

tC<sup>o</sup> 1,3-diaza-2-oxophenoxazine

pols DNA polymeraseswt wild-type RB69pol

RB69pol bacteriophage RB69 DNA polymerase
 KF Escherichia coli DNA polymerase I
 NBP <u>n</u>ascent base-pair <u>b</u>inding <u>p</u>ocket

**dAP** 2-aminopurine

Pu purinePy pyrimidine

Cα-H methylene hydrogen atom of GlydNMP deoxynucleoside monophosphatedNTP deoxynucleoside triphosphate

 $k_{\mathrm{obs}}$  observed rate constant

 $k_{pol}$  maximum rate of dNMP insertion

 $K_{d,app}$  [dNTP] that supports the half-maximal rate of dNMP insertion

**P/T** primer-template DNA duplex

#### References

- Kathe SD, Barrantes-Reynolds R, Jaruga P, Newton MR, Burrows CJ, Bandaru V, Dizdaroglu M, Bond JP, Wallace SS. Plant and fungal Fpg homologs are formamidopyrimidine DNA glycosylases but not 8-oxoguanine DNA glycosylases. DNA Repair (Amst). 2009; 8:643–653. [PubMed: 19217358]
- Steenken S, Jovanovic SV. How Easily Oxidizable Is DNA?. One-Electron Reduction Potentials of Adenosine and Guanosine Radicals in Aqueous Solution. J Am Chem Soc. 1997; 119:617–618.
- 3. Sekiguchi M, Tsuzuki T. Oxidative nucleotide damage: consequences and prevention. Oncogene. 2002; 21:8895–8904. [PubMed: 12483507]
- 4. Malins DC, Haimanot R. Major alterations in the nucleotide structure of DNA in cancer of the female breast. Cancer Res. 1991; 51:5430–5432. [PubMed: 1655250]
- 5. Degan P, Shigenaga MK, Park EM, Alperin PE, Ames BN. Immunoaffinity isolation of urinary 8-hydroxy-2'-deoxyguanosine and 8-hydroxyguanine and quantitation of 8-hydroxy-2'-

deoxyguanosine in DNA by polyclonal antibodies. Carcinogenesis. 1991; 12:865–871. [PubMed: 2029751]

- Steenken S, Jovanovic SV, Bietti M, Bernhard K. The Trap Depth (in DNA) of 8-Oxo-7,8-dihydro-2'deoxyguanosine as Derived from Electron-Transfer Equilibria in Aqueous Solution. J AmChem Soc. 2000; 122:2372–2374.
- 7. Yanagawa H, Ogawa Y, Ueno M. Redox ribonucleosides. Isolation and characterization of 5-hydroxyuridine, 8-hydroxyguanosine, and 8-hydroxyadenosine from Torula yeast RNA. J Biol Chem. 1992; 267:13320–13326. [PubMed: 1618833]
- 8. Berger M, Anselmino C, Mournet JF, Cadet J. High performance liquid chromatographyelectrochemical assay for monitoring the formation of 8-oxo-7,8-dihydroadenine and its related 2′deoxyribonucleoside. J Liq Chromatogr. 1990; 13:929–940.
- Burrows CJ, Muller JG, Kornyushyna O, Luo W, Duarte V, Leipold MD, David SS. Structure and potential mutagenicity of new hydantoin products from guanosine and 8-oxo-7,8-dihydroguanine oxidation by transition metals. EnvironHealth Perspect. 2002; 110(Suppl 5):713-717.
- Luo W, Muller JG, Rachlin EM, Burrows CJ. Characterization of hydantoin products from oneelectron oxidation of 8-oxo-7,8-dihydroguanosine in a nucleoside model. ChemRes Toxicol. 2001; 14:927–938.
- Aller P, Ye Y, Wallace SS, Burrows CJ, Doublie S. Crystal structure of a replicative DNA polymerase bound to the oxidized guanine lesion guanidinohydantoin. Biochemistry. 2010; 49:2502–2509. [PubMed: 20166752]
- 12. Mishchuk YR, Potyagaylo DM, Hovorun DM. Structure and dynamics of 6-azacytidine by MNDO/H quantum-chemical method. J MolStruct. 2000; 552:283–289.
- 13. Verdolino V, Cammi R, Munk BH, Schlegel HB. Calculation of pKa values of nucleobases and the guanine oxidation products guanidinohydantoin and spiroiminodihydantoin using density functional theory and a polarizable continuum model. J PhysChem B. 2008; 112:16860–16873.
- David SS, O'Shea VL, Kundu S. Base-excision repair of oxidative DNA damage. Nature. 2007;
   447:941–950. [PubMed: 17581577]
- Kornyushyna O, Berges AM, Muller JG, Burrows CJ. In vitro nucleotide misinsertion opposite the oxidized guanosine lesions spiroiminodihydantoin and guanidinohydantoin and DNA synthesis past the lesions using *Escherichia coli* DNA polymerase I (Klenow fragment). Biochemistry. 2002; 41:15304–15314. [PubMed: 12484769]
- 16. Kornyushyna O, Burrows CJ. Effect of the oxidized guanosine lesions spiroiminodihydantoin and guanidinohydantoin on proofreading by *Escherichia coli* DNA polymerase I (Klenow fragment) in different sequence contexts. Biochemistry. 2003; 42:13008–13018. [PubMed: 14596616]
- 17. Duarte V, Muller JG, Burrows CJ. Insertion of dGMP and dAMP during in vitro DNA synthesis opposite an oxidized form of 7,8-dihydro-8-oxoguanine. Nucleic Acids Res. 1999; 27:496–502. [PubMed: 9862971]
- Tano K, Iwamatsu Y, Yasuhira S, Utsumi H, Takimoto K. Increased base change mutations at G:C pairs in *Escherichia coli* deficient in endonuclease III and VIII. J Radiat Res. 2001; 42:409–413. [PubMed: 11951664]
- 19. Takimoto K, Tano K, Hashimoto M, Hori M, Akasaka S, Utsumi H. Delayed transfection of DNA after riboflavin mediated photosensitization increases G:C to C:G transversions of supF gene in Escherichia coli mutY strain. Mutat Res. 1999; 445:93–98. [PubMed: 10521694]
- 20. Akasaka S, Takimoto K. Hydrogen peroxide induces G:C to T:A and G:C to C:G transversions in the supF gene of Escherichia coli. Mol Gen Genet. 1994; 243:500–505. [PubMed: 8208241]
- 21. Mcbride TJ, Schneider JE, Floyd RA, Loeb LA. Mutations induced by methylene blue plus light in single-stranded M13mp2. Proc Natl Acad Sci USA. 1992; 89:6866–6870. [PubMed: 1495976]
- Schulz I, Mahler H-C, Boiteux S, Epe B. Oxidative DNA base damage induced by singlet oxygen and photosensitization: recognition by repair endonucleases and mutagenicity. Mutat Res. 2000; 461
- 23. Garrigue-Antar L, Munoz-Antonia T, Antonia SJ, Gesmonde J, Vellucci VF, Reiss M. Missense mutations of the transforming growth factor beta type II receptor in human head and neck squamous carcinoma cells. Cancer Res. 1995; 55:3982–3987. [PubMed: 7664267]

24. Kino K, Sugiyama H. UVR-induced G-C to C-G transversions from oxidative DNA damage. MutatRes. 2005; 571:33–42.

- 25. Hailer MK, Slade PG, Martin BD, Rosenquist TA, Sugden KD. Recognition of the oxidized lesions spiroiminodihydantoin and guanidinohydantoin in DNA by the mammalian base excision repair glycosylases NEIL1 and NEIL2. DNA Repair (Amst). 2005; 4:41–50. [PubMed: 15533836]
- Zhao X, Krishnamurthy N, Burrows CJ, David SS. Mutation versus repair: NEIL1 removal of hydantoin lesions in single-stranded, bulge, bubble, and duplex DNA contexts. Biochemistry. 2010; 49:1658–1666. [PubMed: 20099873]
- 27. Krishnamurthy N, Zhao X, Burrows CJ, David SS. Superior removal of hydantoin lesions relative to other oxidized bases by the human DNA glycosylase hNEIL1. Biochemistry. 2008; 47:7137–7146. [PubMed: 18543945]
- 28. Wang TS, Wong SW, Korn D. Human DNA polymerase α: predicted functional domains and relationships with viral DNA polymerases. FASEB J. 1989; 3:14–21. [PubMed: 2642867]
- 29. Beckman J, Wang M, Blaha G, Wang J, Konigsberg WH. Substitution of Ala for Tyr567 in RB69 DNA polymerase allows dAMP to be inserted opposite 7,8-dihydro-8-oxoguanine. Biochemistry. 2010; 49:4116–4125. [PubMed: 20411947]
- Zhang H, Rhee C, Bebenek A, Drake JW, Wang J, Konigsberg W. The L561A substitution in the nascent base-pair binding pocket of RB69 DNA polymerase reduces base discrimination. Biochemistry. 2006; 45:2211–2220. [PubMed: 16475809]
- 31. Kuchta RD, Mizrahi V, Benkovic PA, Johnson KA, Benkovic SJ. Kinetic mechanism of DNA polymerase I (Klenow). Biochemistry. 1987; 26:8410–8417. [PubMed: 3327522]
- 32. Maniatis, T.; Fritsch, EF.; Sambrook, J. Molecular Cloning. Cold Spring Harbor Laboratory; Cold Spring Harbor, NY: 1982.
- 33. Otwinowski, Z.; Minor, W. Processing of X-ray diffraction data collected in oscillation mode. In: Carter, CW.; Sweet, RM., editors. Methods Enzymol. 1997. p. 307-326.
- 34. Franklin MC, Wang J, Steitz TA. Structure of the replicating complex of a pol α family DNA polymerase. Cell. 2001; 105:657–667. [PubMed: 11389835]
- 35. Murshudov GN, Vagin AA, Dodson EJ. Refinement of macromolecular structures by the maximum-likelihood method. Acta Cryst. 1997; D53:240–255.
- Navaza J. AMoRE: An automated package for molecular replacement. Acta Cryst. 1994;
   A50:157–163.
- Emsley P, Cowtan K. Coot: model-building tools for molecular graphics. Acta Cryst. 2004;
   D60:2126–2132.
- 38. Carson M. Ribbons 2.0. J ApplCryst. 1991; 24:958-961.
- 39. Zhang H, Beckman J, Wang J, Konigsberg W. RB69 DNA polymerase mutants with expanded nascent base-pair-binding pockets are highly efficient but have reduced base selectivity. Biochemistry. 2009; 48:6940–6950. [PubMed: 19522539]
- 40. Aller P, Rould MA, Hogg M, Wallace SS, Doublie S. A structural rationale for stalling of a replicative DNA polymerase at the most common oxidative thymine lesion, thymine glycol. ProcNatl Acad Sci USA. 2007; 104:814–818.
- 41. Stengel G, Purse BW, Wilhelmsson LM, Urban M, Kuchta RD. Ambivalent incorporation of the fluorescent cytosine analogues tC and tC<sup>o</sup> by human DNA polymerase α and Klenow fragment. Biochemistry. 2009; 48:7547–7555. [PubMed: 19580325]
- 42. Hollenstein M, Hipolito CJ, Lam CH, Perrin DM. A self-cleaving DNA enzyme modified with amines, guanidines and imidazoles operates independently of divalent metal cations (M<sup>2+</sup>). Nucleic Acids Res. 2009; 37:1638–1649. [PubMed: 19153138]
- 43. Cahova H, Havran L, Brazdilova P, Pivonkova H, Pohl R, Fojta M, Hocek M. Aminophenyl- and nitrophenyl-labeled nucleoside triphosphates: synthesis, enzymatic incorporation, and electrochemical detection. Angew ChemInt Ed Engl. 2008; 47:2059–2062.
- 44. Liu HB, Gao JM, Maynard L, Saito YK, Kool ET. Toward a New Genetic System with Expanded Dimensions: Size-Expanded Analogues of Deoxyadenosine and Thymidine. J AmChem Soc. 2004; 126:1102–1109.
- 45. Horhota AT, Szostak JW, McLaughlin LW. Glycerol nucleoside triphosphates: synthesis and polymerase substrate activities. Org Lett. 2006; 8:5345–5347. [PubMed: 17078714]

46. Xia G, Chen L, Sera T, Fa M, Schultz PG, Romesberg FE. Directed evolution of novel polymerase activities: mutation of a DNA polymerase into an efficient RNA polymerase. Proc NatlAcad Sci USA. 2002; 99:6597–6602.

- 47. Ghadessy FJ, Ramsay N, Boudsocq F, Loakes D, Brown A, Iwai S, Vaisman A, Woodgate R, Holliger P. Generic expansion of the substrate spectrum of a DNA polymerase by directed evolution. NatBiotechnol. 2004; 22:755–759.
- 48. Loakes D, Holliger P. Polymerase engineering: towards the encoded synthesis of unnatural biopolymers. Chem Commun (Camb). 2009:4619–4631. [PubMed: 19641798]
- Krishnamurthy N, Muller JG, Burrows CJ, David SS. Unusual structural features of hydantoin lesions translate into efficient recognition by Escherichia coli Fpg. Biochemistry. 2007; 46:9355– 9365. [PubMed: 17655276]
- 50. Bren U, Martinek V, Florian J. Free energy simulations of uncatalyzed DNA replication fidelity: structure and stability of T.G and dTTP. G terminal DNA mismatches flanked by a single dangling nucleotide. J Phys Chem B. 2006; 110:10557–10566. [PubMed: 16722767]
- 51. Fagan PA, Fabrega C, Eritja R, Goodman MF, Wemmer DE. NMR study of the conformation of the 2-aminopurine:cytosine mismatch in DNA. Biochemistry. 1996; 35:4026–4033. [PubMed: 8672436]
- 52. Sowers LC, Boulard Y, Fazakerley GV. Multiple structures for the 2-aminopurine-cytosine mispair. Biochemistry. 2000; 39:7613–7620. [PubMed: 10858312]
- 53. Sowers LC, Fazakerley GV, Eritja R, Kaplan BE, Goodman MF. Base pairing and mutagenesis: observation of a protonated base pair between 2-aminopurine and cytosine in an oligonucleotide by proton NMR. ProcNatl Acad Sci USA. 1986; 83:5434–5438.
- 54. Minnick DT, Liu L, Grindley ND, Kunkel TA, Joyce CM. Discrimination against purine-pyrimidine mispairs in the polymerase active site of DNA polymerase I: a structural explanation. ProcNatl Acad Sci USA. 2002; 99:1194–1199.
- 55. Yoshida K, Tosaka A, Kamiya H, Murate T, Kasai H, Nimura Y, Ogawa M, Yoshida S, Suzuki M. Arg660Ser mutation in Thermus aquaticus DNA polymerase I suppresses T-->C transitions: implication of wobble base pair formation at the nucleotide incorporation step. Nucleic Acids Res. 2001; 29:4206–4214. [PubMed: 11600709]
- Freisinger E, Grollman AP, Miller H, Kisker C. Lesion (in)tolerance reveals insights into DNA replication fidelity. EMBO J. 2004; 23:1494–1505. [PubMed: 15057282]
- 57. Kincaid K, Beckman J, Zivkovic A, Halcomb RL, Engels JW, Kuchta RD. Exploration of factors driving incorporation of unnatural dNTPS into DNA by Klenow fragment (DNA polymerase I) and DNA polymerase α. Nucleic Acids Res. 2005; 33:2620–2628. [PubMed: 15879351]
- 58. Beckman J, Kincaid K, Hocek M, Spratt T, Engels J, Cosstick R, Kuchta RD. Human DNA polymerase α uses a combination of positive and negative selectivity to polymerize purine dNTPs with high fidelity. Biochemistry. 2007; 46:448–460. [PubMed: 17209555]
- 59. Morales JC, Kool ET. Functional hydrogen-bonding map of the minor groove binding tracks of six DNA polymerases. Biochemistry. 2000; 39:12979–12988. [PubMed: 11041863]
- 60. Matsuda S, Leconte AM, Romesberg FE. Minor groove hydrogen bonds and the replication of unnatural base pairs. J AmChem Soc. 2007; 129:5551–5557.
- 61. Matsuda S, Romesberg FE. Optimization of interstrand hydrophobic packing interactions within unnatural DNA base pairs. J AmChem Soc. 2004; 126:14419–14427.
- 62. Yang G, Wang J, Konigsberg W. Base selectivity is impaired by mutants that perturb hydrogen bonding networks in the RB69 DNA polymerase active site. Biochemistry. 2005; 44:3338–3346. [PubMed: 15736944]

**Figure 1.**8-oxoG compared with its oxidized products Gh and Sp. **A.** Structures of an incoming dCTP or dATP paired opposite a templating 8-oxoG. **B.** Hydantoin products of one-electron oxidation of 8-oxoG, Gh and Sp, via a 5-OH-8-oxoG intermediate. **C.** Slight rotation of Gh relative to the 2′-deoxyribose sugar (indicated with a curved arrow) forms a base-pair with dATP with Gh in a "*high-syn*" conformation. Note how the base-pair "buckles" (the arrows pointing away from the Gh sugar indicate that the backbone continues in the 5′ and 3′ directions). **D.** Numbering scheme of Gh, shown in the *R*-configuration at C-4.

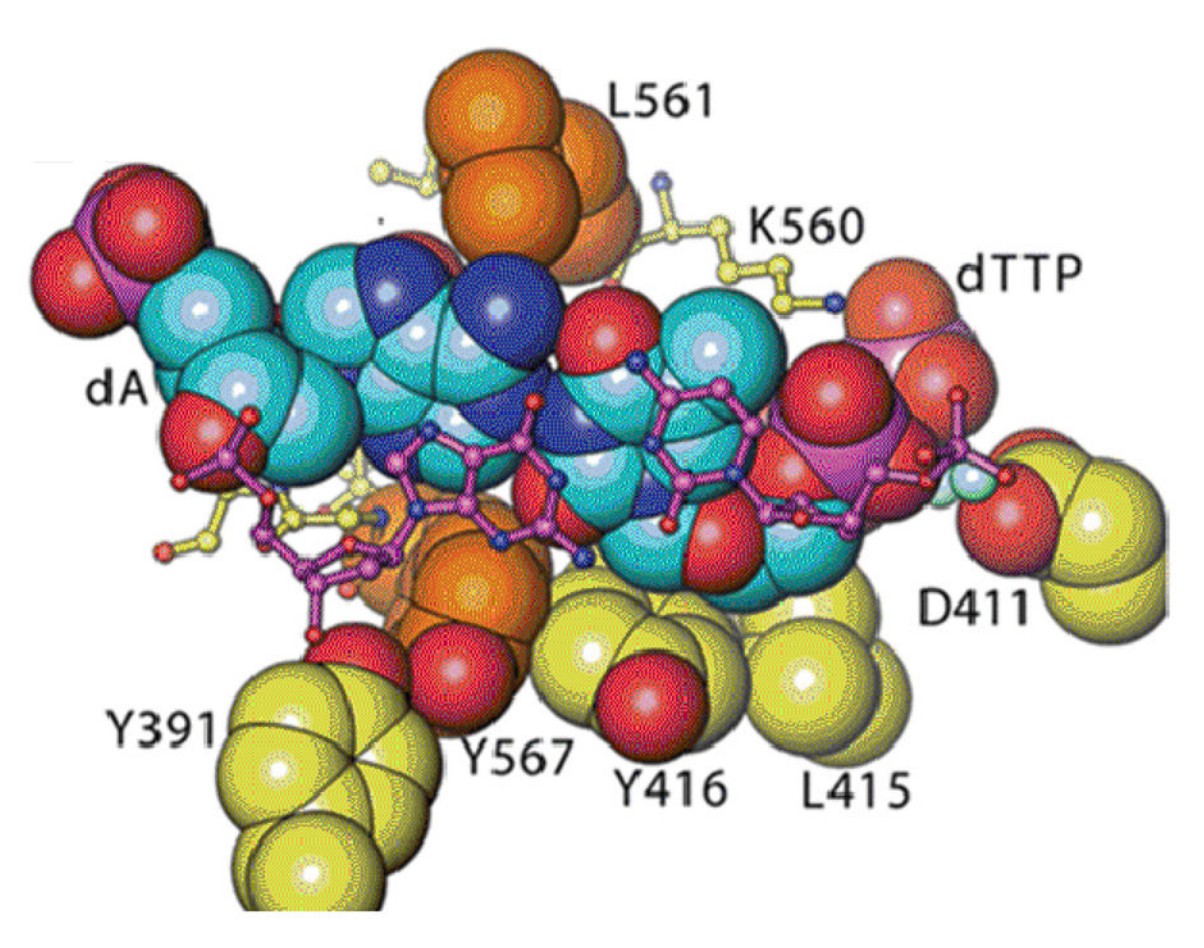


Figure 2. Steric relationship of some of the NBP residues surrounding an incoming dTTP paired opposite a templating dA (from ref (34), PDB entry 1IG9). The nascent base-pair and surrounding residues are shown from the duplex side of the primer-template in space-filling form. The nascent base-pair is shown in blue, and the terminal C:G base-pair, with C located at the primer-terminus, is shown in stick form (purple) for the sake of clarity. L561 and Y567 are colored orange.

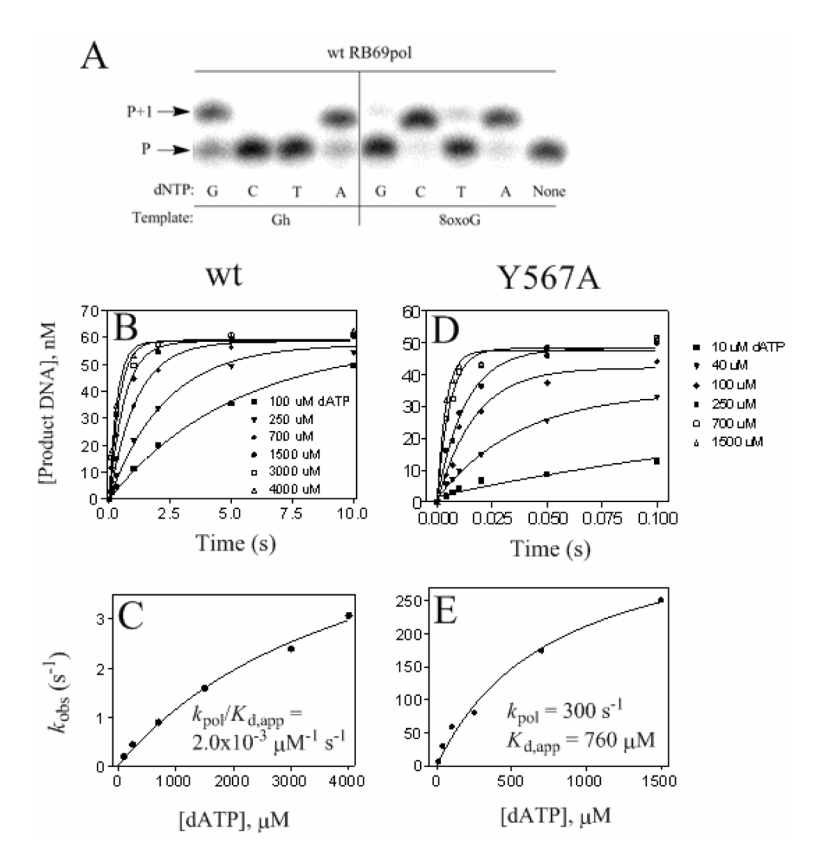


Figure 3. Kinetics of dNMP insertion by wt RB69pol and the Y567A mutant. **A.** Insertion of dNMPs opposite Gh and 8-oxoG by wt RB69pol. P represents the primer, and P+1 represents the primer extended by one nucleotide. Oxidation of 8-oxoG  $\rightarrow$  Gh results in dramatically reduced incorporation of dCMP, to the point that it cannot be observed. **B.** Kinetics of insertion of dAMP opposite Gh by wt. Progress curves at various [dATP]s fit to single-exponential equations. **C.** Plot of  $k_{\rm obs}$  vs [dATP] fit to eq 2. **D.** Kinetics of insertion of dAMP opposite Gh by the Y567A mutant. Same as panel **B** but with data obtained using the Y567A mutant. **E.** Same as panel **C** using the results in panel **D**.

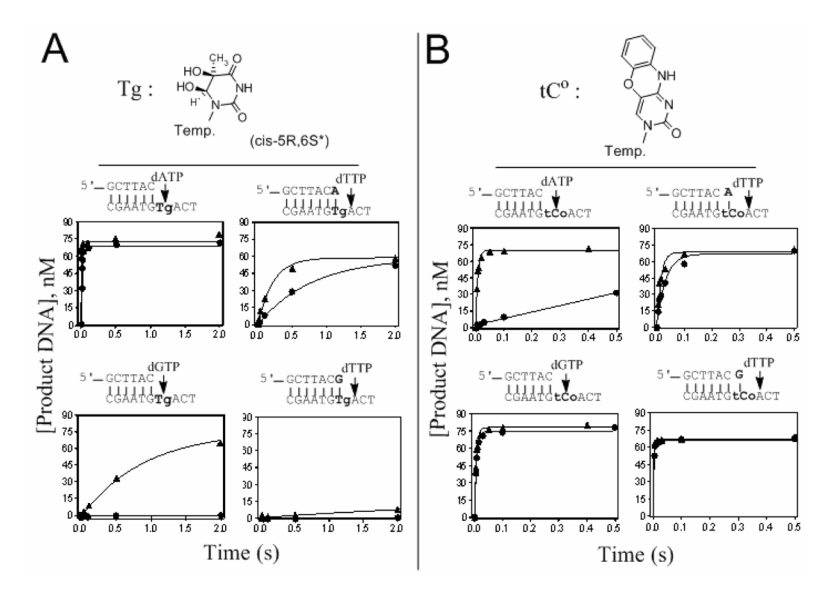


Figure 4.
Progress curves showing the rates of bypass of thymine glycol (Tg) and 1,3-diaza-2-oxophenoxazine (tC°) by wt RB69pol and the Y567A mutant. For reference, P/T sequences and structures of the analogs are shown. Progress curves for insertion of dNMPs were obtained under single turnover conditions without trap DNA, and with 1 mM dNTPs (see Experimental Procedures). A. Rate of DNA product formation for insertion of dAMP and dGMP opposite Tg, and the rate of extension past A:Tg and G:Tg base-pairs (via insertion of dTMP, the next correct dNMP), by wt RB69pol (●) and the Y567A mutant (▲). B. Rate of DNA product formation for insertion of dAMP and dGMP opposite tC°, and extension past A:tC° and G:tC° base-pairs, by wt RB69pol (●) and the Y567A mutant (▲). \* After oligonucleotide synthesis and deprotection, Tg is predominantly in the cis-5R,6S configuration (40).

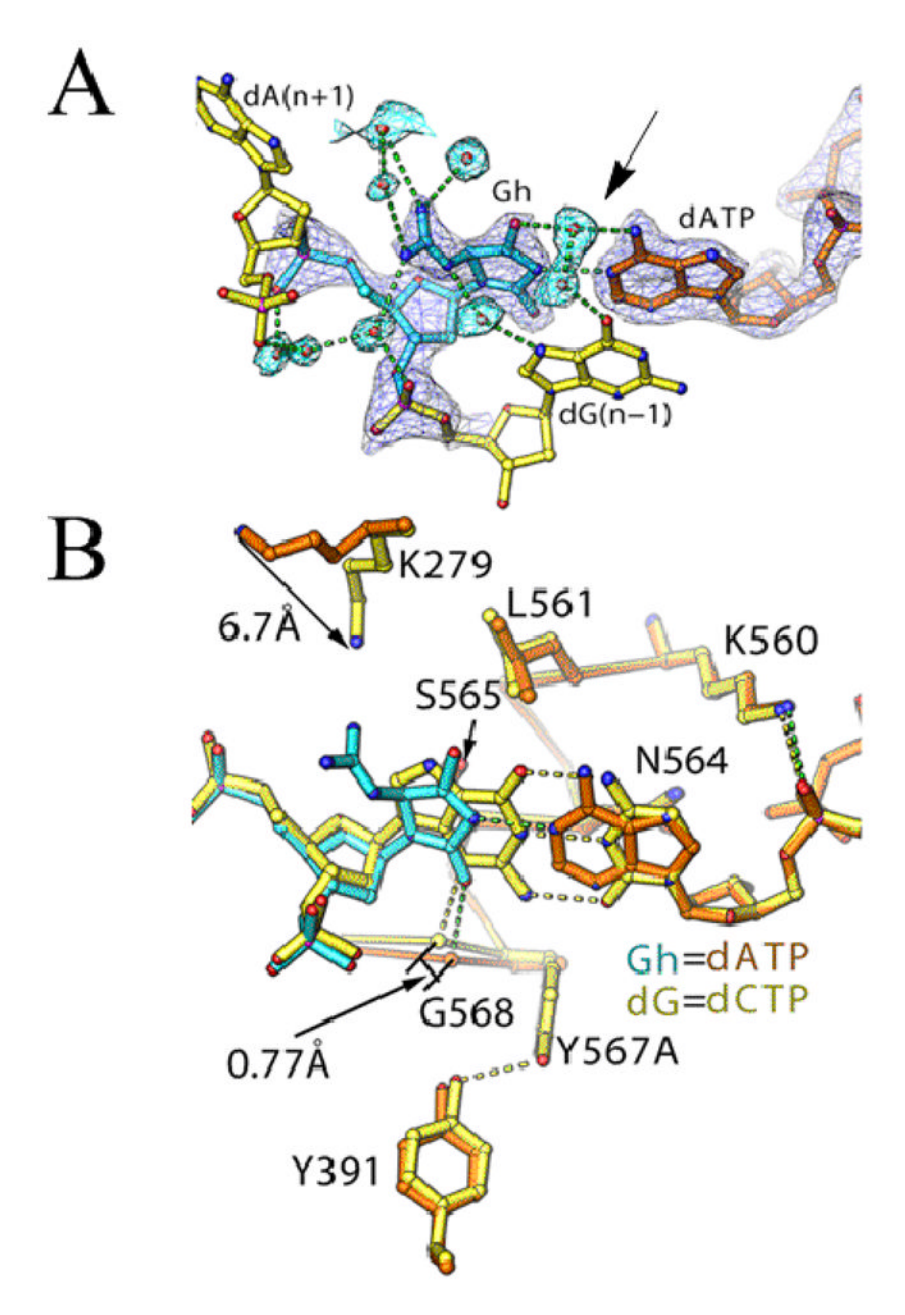
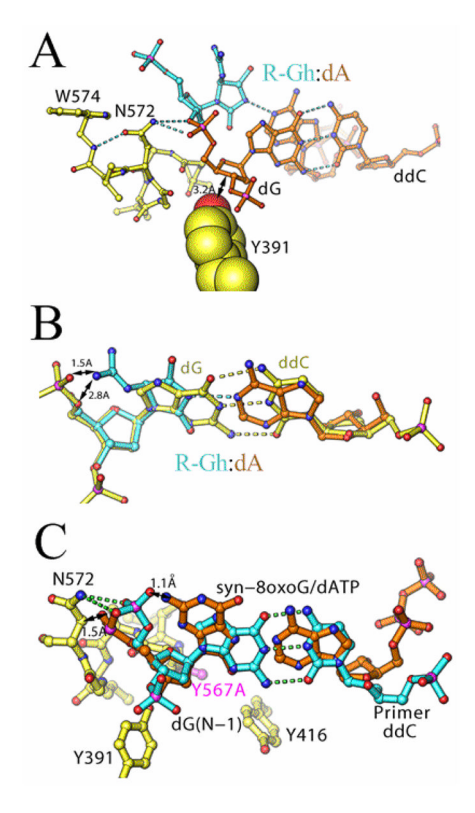


Figure 5.

Crystal structure of the RB69pol Y567A mutant in a complex with a dATP:Gh base-pair and its relationship to residues in the NBP. **A.** Omitted Fo-Fc electron density map of the dATP:Gh nascent base-pair. Note the number of water molecules that surround the guanidinium group, and the water-mediated hydrogen bonding network that links Gh and dATP (pointed to with an arrow). **B.** Comparison of the crystal structures of wt and the Y567A mutant in a complex with dCTP:dG and dATP:Gh base-pairs, respectively. Superimposed palm domains show that the Y567A substitution resulted in a shift of G568 into the DNA minor-groove by ~0.8 Å. The wt:dCTP:dG backbone and base-pair is colored yellow, and the Y567A:dATP:Gh backbone is colored orange. The dCTP:dG base-pair is shown in yellow, and the dATP:Gh base-pair is shown with dATP colored orange, and Gh colored blue.

**Figure 6.**Possible "wobble" configurations of the dTTP:dG and dATP:Gh mispairs in the Y567A mutant complex. **A.** Downward shift of dG into the DNA minor groove on the templating side (against G568) leads to a "wobble" base-pair between dG and dTTP. **B.** Downward shift of dGTP into the DNA minor groove into the space provided by the Y567 to A substitution leads to an "inverted wobble" base-pair between dGTP and Gh.



**Figure 7.** *In silico* modeling of dAMP:Gh as a terminal (n-1) base-pair and its relationship to surrounding amino acid side-chains in the Y567A mutant. **A.** The terminal base-pair ddC:dG in the Y567A:dATP:Gh structure (orange) and the hydrogen bonding network it forms between the 5'-bridging phosphate of dG and side-chains N572 and W574. **B.** Superposition of the glycosidic bonds of the dATP:Gh base-pair onto the ddC:dG base-pair. Black arrows denote unfavorable interactions. **C.** Superposition of the dATP:*syn*-8-oxoG base-pair onto the ddC:dG base-pair. Black arrows denote unfavorable interactions (29). Note that both Gh and *syn*-8-oxoG form unfavorable contacts with their 5'-terminal phosphates.

Table 1

Primer-template sequences used in this study\*.

GCGGACTGCTTAC-dd              GCGCCTGACGAATG <b>G<sub>h</sub></b> ACT	${ m D_{GH}}^{ m dd}$
GCGGACTGCTTAC IIIIIIIIIII GCGCCTGACGAATG <b>X</b> ACT	$\mathbf{D}_{\mathbf{x}}$ (X = Gh, 8-oxoG, Tg, or tC°)
GCGGACTGCTTACC GCGCCTGACGAATGG <sub>O</sub> <b>A</b> CT	$\mathbf{D}_{\mathbf{C:OG}}$
GCGGACTGCTTACA IIIIIIIIIIIIIII GCGCCTGACGAATGX <b>A</b> CT	$\mathbf{D}_{A:X}$ (X = Gh, 8-oxoG, Tg, or tC <sup>o</sup> )
GCGGACTGCTTACG IIIIIIIIIIII GCGCCTGACGAATGX <b>A</b> CT	$\mathbf{D}_{\mathbf{G}:\mathbf{X}}$ (X = Gh, Tg, or tC°)

<sup>\*</sup> The templating base is in bold.  $G_O = 8$ -oxoG, and  $G_h =$  guanidinohydantoin (Gh).  $D_{GH}^{dd}$  was used to grow crystals of the ternary complex.

NIH-PA Author Manuscript

Table 2

pe RB69pol and its Y567A mutant.

Beckman et al.

Enzyme	dNTP	Template	$\textit{k}_{pol}  (s^{-1})$	$K_{ m d,app}~(\mu  m M)$	Enzyme dNTP Template $k_{\rm pol}~(\rm s^{-1})~K_{\rm dapp}~(\mu M)~k_{\rm pol}/K_{\rm d,app}~(\mu M^{-1}~\rm s^{-1})$
Wild Type dATP <sup>a</sup>	dATPa	Gh	qON	qON	$NDb = 2.0 \times 10^{-3}$
	dCTP	පි	$^{Q}$	$ND^b$	$ND^b = 5.7 \times 10^{-5}$
Y567A	dATP	g	300	760	760 0.39
	dGTP	É	8.4	1400	$1400   3.4 \times 10^{-3}$

<sup>a</sup>Progress curves were biphasic. Values shown were from the fast phase which comprised 80% of the product formed (see text).

 $^{b}$ ND = Not  $_{c}$ Determined because the value of  $K_{d,app}$  was too high (> 2 mM). The  $k_{pol}/K_{d,app}$  second order value was obtained by calculating the slope of a linear line fitted to the data: y = mx + b, where  $m = slope = \Delta k_0 bs/\Delta [dNTP] = k_{pol}/Kd$ , app. Of the values shown, standard deviations were within 10–20% and ~30% for  $k_{pol}$  and Kd, app values, respectively. Page 21

Table 3

Crystallographic Data and Refinement Statistics

Mutant         Y567A           Ternary complex with:         dATP:Gh           Space group $P2_12_12_1$ Unit cell dimensions [a, b, c(Å)] $75.013,119.783,130.727$ Resolution range (Å) <sup>a</sup> $50.00-2.00 (2.07-2.00)$ Wavelength (Å) $1.10000$ Number of reflections $74483 (5982)$
Space group         P2 <sub>1</sub> 2 <sub>1</sub> 2 <sub>1</sub> Unit cell dimensions [a, b, c(Å)]         75.013,119.783,130.727           Resolution range (Å) <sup>a</sup> 50.00-2.00 (2.07-2.00)           Wavelength (Å)         1.10000           Number of reflections
Unit cell dimensions [a, b, c(Å)] 75.013,119.783,130.727  Resolution range (Å) <sup>a</sup> 50.00-2.00 (2.07-2.00)  Wavelength (Å) 1.10000  Number of reflections
Resolution range (Å) $^a$ 50.00-2.00 (2.07-2.00)  Wavelength (Å) 1.10000  Number of reflections
Wavelength (Å) 1.10000  Number of reflections
Number of reflections
Unique 74483 (5982)
7.100 (2702)
Redundancy 4.5 (3.2)
Completement (%) 93.2 (75.8)
$R_{\text{merge}}(\%)b$ 7.8 (>100)
Ι/σ 14.3 (0.96)
Refinement statistics
Reflections 69794
$R_{\text{work}}$ (%) <sup>C</sup> 19.4
$R_{free}$ (%) $^d$ 23.1
Final model
Non-hydrogen atoms 8925
Amino acid residues 903
Water molecules 705
$Ca^{2+}$ ions 4
Template nucleotides 18
Primer nucleotides 13
dNTP molecules 1
Average B-factors (Ų)
Protein 27.3
Waters 34.3
<u>r.m.s.d.</u> <sup>e</sup>
Bond length (Å) 0.0069
Bond angles (°) 1.106
PDB accession ID 3NAE

 $<sup>^{</sup>a}$ The highest resolution shell statistics are in parenthesis.

 $<sup>{}^</sup>bR_{merge} = <\Sigma_{hkl}\Sigma_{j}|I_{f}(hkl) - < I(hkl) > | > / < I(hkl) > , \text{ merging statistics for all symmetry-mates}.$ 

 $c_{\text{RWork}} = \Sigma_{hkl} |F_{\text{Obs}}(hkl) - F_{\text{calc}}(hkl)|/\Sigma_{hkl}|F_{\text{Obs}}(hkl)$ , crystallographic R-factor.

 $d_{\mbox{Rfree}}$ : Cross-validation R-factor for ~5% of the total unique reflections that have been randomly selected.

 $<sup>\</sup>begin{array}{c} e \\ {\rm r.m.s.d.: root\text{-}mean\text{-}square deviation from ideal values.} \end{array}$ 

Table 4

Kinetic parameters for insertion of correct dNMPs past terminal base-pairs containing Gh or 8-oxoG.

Beckman et al.

ı		1			
Α	$k_{ m pol}/K_{ m d,app}~(\mu { m M}^{-1}~{ m s}^{-1}$	1700 $3.9 \times 10^{-5} b$	$ND^a = 4.6 \times 10^{-5} b$	0.31	740 0.24
Y567A	<i>К</i> <sub>d,арр</sub> (µМ)	1700	$ND^a$	850	740
	$k_{\rm pol}~({ m s}^{-1})$	0.067	$ND^a$	200	230
9pol	$k_{\rm pol}  ({\rm s}^{-1}) - K_{\rm dapp}  (\mu {\rm M}) - k_{\rm pol} / K_{\rm dapp}  (\mu {\rm M}^{-1}  {\rm s}^{-1}) - k_{\rm pol}  ({\rm s}^{-1}) - K_{\rm dapp}  (\mu {\rm M}) - k_{\rm pol} / K_{\rm dapp}  (\mu {\rm M}^{-1}  {\rm s}^{-1})$	$1.3 \times 10^{-5} b$	$1.6\times 10^{-6}b$	$1.2\times 10^{-2}b$	$5.0  imes 10^{-3}  b$
wt RB69pol	$K_{ m d,app}$ ( $\mu{ m M}$ )	$ND^a$	$^{p}$ ON	$ND^a$	$ND^a$
	$k_{\rm pol}~({ m s}^{-1})$	$ND^a$	$ND^a$	$ND^a$	$D_{C:OG}^c$ $ND^a$
	P/T	dTTP D <sub>A:GH</sub>	$D_{G:GH}$	$\mathrm{D}_{\mathrm{A:OG}}^{\mathcal{C}}$ ND $^a$	$\mathrm{D}_{\mathrm{C}:\mathrm{OG}}^{\mathcal{C}}$
	dNTP	dTTP			

 $^{2}$ ND = Not <u>Determined because</u> the value of *K*d, app was too high (> 2 mM).

 $b_{p} = k_{pol}/K_{d,app}$  second order value was obtained by calculating the slope of a linear line fitted to the data: y = mx + b (see Table 2).

Cata obtained previously (29). Standard deviations were within the same range as the data presented in Table 2.

Page 23